HHS Public Access

Author manuscript

J Physiol. Author manuscript; available in PMC 2022 May 01.

Published in final edited form as:

J Physiol. 2021 November ; 599(22): 5047–5060. doi:10.1113/JP281717.

Selective glycinergic input from vGluT3 amacrine cells confers a suppressed-by-contrast trigger feature in a subtype of M1 ipRGCs in the mouse retina

Seunghoon Lee[1,*], **Minggang Chen**[1,*], **Yuelin Shi**[1], **Z. Jimmy Zhou**[1,2,3]

[1]Department of Ophthalmology and Visual Science, Yale University School of Medicine, New Haven, CT, USA

[2]Department of Cellular and Molecular Physiology, Yale University School of Medicine, New Haven, CT, USA

[3]Department of Neuroscience, Yale University School of Medicine, New Haven, CT, USA

Abstract

The M1 type ipRGC (intrinsically photosensitive retinal ganglion cell) is known to encode ambient light signals for non-image-forming visual functions such as circadian photo-entrainment and the pupillary light reflex. Here, we report that a subpopulation of M1 cells (M1a) in the mouse retina possess the suppressed-by-contrast (sbc) trigger feature that is a receptive field property previously found only in ganglion cells mediating image-forming vision. Using optogenetics and the dual patch clamp technique, we found that vesicular glutamate transporter 3 (vGluT3) (vGluT3) amacrine cells make glycinergic, but not glutamatergic, synapses specifically onto M1a cells. The spatiotemporal and pharmacological properties of visually evoked responses of M1a cells closely matched the receptive field characteristics of vGluT3 cells, suggesting a major role of the vGluT3 amacrine cell input in shaping the sbc trigger feature of M1a cells. We found that the other subpopulation of M1 cells (M1b), which did not receive a direct vGluT3 cell input, lacked the sbc trigger feature, being distinctively different from M1a cells in intrinsic photo responses, membrane excitability, receptive-field characteristics and morphological features. Together, the results reveal a retinal circuit that uses the sbc trigger feature to regulate irradiance coding and potentially send image-forming cues to non-image-forming visual centres in the brain.

Corresponding author Z. J. Zhou: 300 George Street, Suite 8100, New Haven, CT 06510, USA. jimmy.zhou@yale.edu.

*These authors contributed equally to this work.

Author contributions

SL and MC performed experiments and analysed results. YS participated in the initial experiments. ZJZ and SL designed experiments, analysed results and wrote the paper.

Competing interests

The authors declare that they have no competing interests.

Supporting information

Additional supporting information can be found online in the Supporting Information section at the end of the HTML view of the article. Supporting information files available:

Peer Review History

Statistical Summary Document

Keywords

circadian entrainment; ipRGC; non-image-forming vision; pupillary reflex; suppressed-by-contrast; vGluT3 amacrine cell

Introduction

Intrinsically photosensitive retinal ganglion cells (ipRGCs) are retinal output neurons that use melanopsin to capture light directly and encode ambient irradiance (Berson *et al.* 2002; Hattar *et al.* 2002; Provencio *et al.* 2002). Among the six types of ipRGCs (M1–M6) found in mice, the M1 type displays the strongest melanopsin-driven photocurrent (Schmidt & Kofuji, 2009; Ecker *et al.* 2010; Zhao *et al.* 2014) and forms major visual pathways to brain regions [e.g. suprachiasmic nucleus (SCN), olivary pretectal nucleus (OPN) and inter-geniculate leaflet] that are known for non-image-forming visual functions, such as photo-entrainment of circadian rhythm and the pupillary light reflex (Gooley *et al.* 2001; Lucas *et al.* 2001; Berson *et al.* 2002; Hannibal *et al.* 2002; Hattar *et al.* 2002; Panda *et al.* 2002; Ruby *et al.* 2002). M1 cells also receive a glutamatergic excitatory synaptic input from bipolar cells (Dacey *et al.* 2005; Perez-Leon *et al.* 2006; Wong *et al.* 2007) and this input is thought to mainly extend the sensitivity profile of M1 cells toward the dim light range (Wong *et al.* 2007). In addition to an excitatory synaptic input, M1 cells have also been reported to receive inhibitory synaptic inputs, presumably from amacrine cells (Perez-Leon *et al.* 2006; Wong *et al.* 2007; Zhao *et al.* 2014); however, the circuitry and function of such inputs have remained obscure. Given that amacrine cells are known to shape the receptive fields (or trigger features) of ganglion cells in image-forming visual pathways, an intriguing question is whether M1 cells acquire any spatiotemporal trigger features from their interactions with amacrine cells and thereby encode any specific image-vision cues.

M1 cells have been reported to consist of subpopulations that differentially express molecular markers such as transcription factors Pou4f2 (Brn3b) and Tbx20 (T-box), as well as Ras guanyl nucleotide-releasing protein 1 (Rasgrp1) (Chen *et al.* 2011; Berg *et al.* 2019). For example, Brn3b-positive M1 cells project to OPN, thus contributing to the pupillary light reflex, whereas Brn3b-negative M1 cells send their axons to SCN, affecting circadian entrainment (Chen *et al.* 2011). However, such molecular distinctions have not yielded recognizable physiological subtypes because the underlying morphological and biophysical parameters so far examined vary widely over orders of magnitude across the cell population without significant covariation, arguing for population encoding, but against the functional subclassification of M1 cells (Emanuel *et al.* 2017; Milner & Do, 2017). It remains to be determined whether a closer examination of a broader array of functional parameters that include, for example, synaptic properties and circuit functions will reveal any hidden M1 subclasses.

In the present study, we found that vesicular glutamate transporter 3 (vGluT3) amacrine cells, which are glutamatergic amacrine cells (GAC) known to co-release glutamate and glycine (Lee *et al.* 2014; Kim *et al.* 2015; Lee *et al.* 2016; Kim & Kerschensteiner, 2017), made selective glycinergic, but not glutamatergic, synapses with a subpopulation of M1

cells. This glycinergic input from GACs was highly sensitive to local contrast and resulted in a suppressed-by-contrast (sbc) receptive field in the targeted M1 subpopulation, revealing a classic trigger feature of image-forming vison in a non-image-forming ganglion cell population. Moreover, the dichotomy in synaptic connectivity between vGluT3 and M1 cells was found to be correlated with distinctive differences in intrinsic photosensitivity, membrane excitability and morphological characteristics of M1 cells, demonstrating the existence of highly stereotypic functional subtypes among M1 cells. A preliminary report of the findings has been made avaiable previously in abstract form (Lee *et al.* 2019a).

Methods

Ethical approval

All animal procedures and experiments were approved by Institutional Animal Care and Use committees (IACUC) at Yale University and were in compliance with National Institutes of Health guidelines.

Animals and *ex vivo* retina preparation

vGluT3-Cre/ChR2-YFP/OPN4-GFP mice (6–12 weeks old, either sex, kept under a 12:12 h light/dark photocycle and fed with food and filtered water *ad libitum* in a Yale University vivarium) were generated by cross-breeding vGluT3-Cre mice (The Jackson Laboratory, Bar Habor, ME, USA; RRID: IMSR_JAX018147) (Grimes *et al.* 2011; Lee *et al.* 2014), ChR2-YFP mice (RRID: IMSR_JAX012569) and OPN4-GFP (Berg *et al.* 2019) (GENSAT, The Rockefeller University, New York, NY, USA; RRID: MMRRC_03 3064-UCD) generously provided by David Berson (Brown University, Providence, USA). Mice were dark-adapted for 1–2 h before being killed with an overdose (0.1 ml, I.P.) of a 10:1 mixture of ketamine (100 mg mL^{-1}; Ketaset, Zoetis Inc., Kalamazoo, MI, USA) and xylazine (100 mg ml^{-1}; AnaSed, Akorn Animal Health, Inc., Lake Forest, IL, USA), followed by decapitation. Retinas were dissected under dim red-light illumination and kept in carbogenated (95% O_2 and 5% CO_2) artificial cerebrospinal fluid (aCSF) (see below) at room temperature (23°C) before recording.

Electrophysiology and two-photon imaging

Electrophysiological recordings and two-photon imaging were performed as described previously (Lee *et al.* 2010; Lee *et al.* 2014; Lee *et al.* 2016; Chen *et al.* 2017). In brief, patch clamp recordings were made in the flat-mount retina in aCSF (composition in mM: 120 NaCl, 3.1 KCl, 1.1 $CaCl_2$, 1.2 $MgCl_2$, 1.25 $MgSO_4$, 26 $NaHCO_3$, 0.5 L-glutamine, 0.1 ascorbic acid, 0.1 Na-pyruvate and 20 glucose) saturated with 95% O_2–5% CO_2 at 32–34°C. Three pipette solutions were used as follows (composition in mM): (1) for voltage clamp, 105 $CsMeSO_4$, 0.5 $CaCl_2$, 10 Hepes, 5 EGTA, 5 Na_2-phosphocreatine, 2 ATP-Mg, 0.5 GTP-2Na, 2 ascorbic acid, 8 QX314-Cl, pH 7.2, with 20–30 CsOH; (2) for current clamp, 105 potassium gluconate, 5 KCl, 0.5 $CaCl_2$, 2 $MgCl_2$, 5 EGTA, 10 Hepes, 5 Na_2-phosphocreatine, 2 ATP-2Na, 0.5 GTP-2Na, 2 ascorbic acid, pH 7.2 with 5 NaOH and 15 KOH; (3) for loose patch clamp, aCSF. Drugs were applied by bath perfusion at the same concentrations as first described in the text (see below). M1 ipRGCs and vGluT3 amacrine cells were targeted for recording based, respectively, on their enhanced green

fluorescent protein (EGFP) and yellow fluorescent protein (YFP) labelling viewed under either brief (2–10 s) flashes of epifluorescence illumination (10^{10} photons $\mu m^{-2}s^{-1}$ at retina, 465 ± 15 nm in wavelength) or two-photon imaging using a 910–920 nm laser (Ti:Sapphire pulsed laser; MaiTai, Newport, CA, USA) in an imaging system (Ultima; Bruker Nano, Inc., Madison, WI, USA) configured on a BX51WI microscope (Olympus, Tokyo, Japan) with a 60×, 1.0 NA objective (LUMPlanFL/IR, Olympus). Recordings were made under IR illumination (750 nm wavelength) and viewed through a CCD camera (CoolSnap HQ; Roper Scientific Inc., Princeton, NJ, USA). All recordings were made between 13.00 h and 19.00 h. Electrophysiological data were recorded with a Multiclamp 700B patch clamp amplifier (Molecular Devices, Sunnyvale, CA, USA), stored on Power Lab (AD Instruments, Colorado Springs, CO, USA) and analysed with pClamp10.2 (Molecular Devices), Origin 9 (Origin Lab Corp., Northampton, MA, USA) and Matlab 2018a (MathWorks, Natick, MA, USA). Liquid junction potentials (10.1 mV between aCSF and the Cs^+-based pipette solution; 8.3 mV between aCSF and the K^+-based pipette solution) were calculated and corrected.

Visual and optogenetic (ChR2) stimulation

Visual stimulus patterns were generated using VisionWorks (Durham, NH, USA) on a black-and-white transmissive LCD display (Sony LCX017 chip, 1024 × 768 pixels, 1.8 inch diagonal, 250:1 contrast ratio; bbs bildund lichtsysteme GmbH, Bad Wiessee, Germany) and projected to the retina via the microscope condenser lens. Image intensity at retina was 1.5×10^4 to 9×10^5 photons $\mu m^{-2}s^{-1}$ with an intensity-weighted mean wavelength of 573 nm). Stable light responses were obtained with 10–15 min of dark adaptation prior to the establishment of a patch clamp configuration.

ChR2 was activated by intense *blue light* from either a high power LED (λ_{peak}, 470 nm) focused on the retina through the condenser lens or from the epifluorescence light source (100 W Hg bulb, band-pass filtered at 465 ± 15 nm, focused on the retina through an 60×, NA/0.9 water immersion objective lens of a BX51WI microscope; Olympus) controlled by a Uniblitz shutter (Vincent Associates, Rochester, NY, USA). The intensity of the *blue light* measured at the retina was 22 nW μm^{-2} (5.5×10^{10} photons μm^{-2} s^{-1}) and 8 nW μm^{-2} (2×10^{10} photons μm^{-2} s^{-1}) for the blue LED and the Hg bulb, respectively. In experiments in which both visual (white light) and optogenetic (blue light) stimuli were tested, optogenetic stimulation was always given after all visual stimulation had been completed aiming to prevent any blue light effect on visual responses (either photoreceptor-mediated or intrinsic).

Chemicals

All pharmacological agents were prepared in ultrapure water or DMSO based on solubility. Hexamethonium (HEX, catalogue no. H0879), CPP (catalogue no. C104), SR95531 (catalogue no. S106) and 18βGA (catalogue no. G10105) were purchased from Millipore Sigma (St Louis, MO, USA). L-AP4 (catalogue no. ALX-550–026-M025) and CNQX (catalogue no. ALX-550–042-M050) were obtained from Enzo Life Sciences (Farmingdale, NY, USA). Strychnine (catalogue no. AC158950250) and Alexa Fluor 594 Hydrazide (catalogue no. A10438) were purchased from Thermo Fisher Scientific (Waltham, MA,

USA). ACET (catalogue no. 2728–10) was purchased from Tocris BioScience (Minneapolis, MN, USA).

Statistical analysis

Spike rates were computed by convolving raster plot with normalized step function with a duration of 0.1 s. All statistical results were expressed as the mean ± SD. Statistical significance was tested by Student's two sample *t* test. $P < 0.05$ was considered statistically significant. For correlation analysis, Spearman's ranked correlation coefficient (ρ) was used based on normality test.

Z-series stacks of two-photon images of fluorescence labelling and whole-cell patch clamped cells (filled with Alexa Fluor 594) in the whole-mount retina were taken under two-photon imaging and processed with Prairie View (Bruker Nano, Inc.), ImageJ (NIH, Bethesda, MD, USA) and custom-made programs using Matlab 2018a (MathWorks). Dendritic density of M1 cells was computed as the number of pixels occupied by dendrites per annulus region (25 μm-thick, Δradius = 25 μm, centred on the soma) divided by the total number of pixels in the annulus area.

Results

Differential synaptic output from GACs to two subtypes of M1 cells

To determine whether M1 cells receive direct synaptic input from GACs, we recorded from M1 cells under whole-cell patch clamp, at the same time as stimulating channel rhodopsin 2 (ChR2)-expressing GACs with a flash of intense, full-field blue light (referred to as *blue light* henceforth) in flat-mount retinas of mice that were generated by crossing OPN4-GFP with vGluT3Cre::ChR2-YFP mice. M1 cells, identified based on their distinctively brighter GFP expression compared to other ipRGC types in this mouse line (Berg *et al.* 2019), were voltage clamped under the condition in which synaptic transmission of light-evoked signals from photoreceptors to bipolar cells was inhibited by an antagonist cocktail containing (in μm) 20 L-AP4, 20 ACET and 300 hexamethonium (added as a precaution to block nicotinic transmission) (Lee *et al.* 2014). We found two dramatically different responses from two distinct subpopulations of M1 cells. The first subpopulation (termed M1a hence force) (Fig. 1A) responded to *blue light* with a robust outward current at 0 mV and a slowly developing inward current at −70 mV ($n = 82$) (Fig. 1C). The second population (M1b) (Fig. 1B) responded to *blue light* with only a slowly developing inward current at −70 mV, but no outward current at 0 mV ($n = 71$) (Fig. 1D). The response differences seen at 0 mV between M1a and M1b cells were not the result of variation in the recording condition or a single M1 cell type showing different properties at different topographic locations of the retina because these responses differences were also observed between neighbouring M1a and M1b cells simultaneously recorded in the same retina to the same *blue light* stimulation ($n = 5$ pairs) (Fig. 1E).

The outward currents in M1a cells were activated within 4–8 ms of the onset of *blue light* (Fig. 1C) and resistant to CNQX (40 μm) + CPP (100 μm) ($n = 12$) (Fig. 1E–G), suggesting a direct inhibitory input from GACs. The slowly activated inward current responses at −70

mV were also resistant to CNQX and CPP in both M1a (n = 3) (Fig. 1E, middle) and M1b cells (data not shown), consistent with melanopsin-mediated intrinsic light responses of M1 cells (Berson *et al*. 2002; Hattar *et al*. 2002; Wong *et al*. 2005; Schmidt *et al*. 2008). Additional pharmacological experiments showed that the *blue light*-evoked outward currents in M1a cells at 0 mV were resistant to the $GABA_A$ receptor antagonist SR95531 (SR) (50 μM, n = 4) and the gap junction blocker 18 βGA (25 μM, n = 5, applied in the presence of the cocktail + CNQX and CPP), but were completely blocked by strychnine (STRY) (1 μM, n = 7) (Fig. 1F and G). Dual patch clamp recording from overlapping GAC and M1a pairs further demonstrated the inhibitory synaptic transmission from a single GAC to a postsynaptic M1a under voltage clamp (n = 2) (Fig. 1I). These results established that GACs made direct glycinergic, but not glutamatergic, synapses onto M1a cells. The differential glycinergic connectivity between GACs and M1 subpopulations thus provided a circuit basis for dividing M1 cells into two broadly defined and distinctive subtypes (Fig. 1H). Notably, we encountered roughly equal numbers of M1a and M1b cells (80 *vs*. 73) (Fig. 1H) in our randomly targeted recordings of M1 cells, suggesting an approximately equal distribution between the two subtypes of GFP-labelled M1 cells in this mouse line.

Receptive field properties of M1a and M1b cells

To understand the receptive field structures of M1a and M1b cells, we recorded the responses of these cells to light spots and annuli of various sizes under voltage clamp and compared these visually evoked responses with the optogenetically (*blue light*) evoked inhibitory inputs from GACs. M1a cells responded to a small centre light spot (25 μm in radius) with a transient outward current at 0 mV and a slowly activated inward current at −70 mV (Fig. 2A). The outward inhibitory current had a larger On and a smaller Off component (Fig. 2A and C). The spatial profile of the On component was slightly broader than that of the Off component (n = 33), although both components were spatially confined within the dendritic field of M1a cells (Fig. 2C), indicating that the light-evoked inhibitory inputs were from small-field amacrine cells. The light-evoked inward current at −70 mV, which had an On polarity and was resistant to L-AP4, had a spatial profile coinciding with the dendritic field of M1a cells, consistent with a melanopsin-mediated intrinsic light response (Fig. 2A and C). Occasionally, we also detected an additional fast inward response at −70 mV (Fig. 2A, inset), which was sensitive to L-AP4, suggestive of a bipolar cell-mediated glutamatergic input. However, this transient input was relatively small and rarely observed when illuminated with light annuli or small light spots (50–100 um in radius) (Fig. 2A, inset). On the other hand, M1b cells responded to a small light spot at 0 mV with either no current, or a very small outward current that had a broader spatial profile (especially for the On component) than the inhibitory input profile of M1as, suggesting a weak input from medium/wide field amacrine cells to M1b cells (Fig. 2B and D). At −70 mV, M1b cells responded to a light spot with a slowly activating inward current for which the spatial profile also coincided with the dendritic fields of the cells, consistent with a melanopsin-mediated intrinsic light response. However, the amplitude of the melanopsin-mediated inward current was significantly smaller in M1b cells (24 ± 10 pA, n = 12) than in M1a cells (76 ± 40 pA, n = 28, P < 0.0001) (Fig. 2A–D and F).

Statistical analysis found a positive correlation between the amplitudes of On and Off components of the small-spot (25–50 μm in radius)-evoked inhibitory inputs to M1as (Spearman's correlation coefficient, $\rho = 0.506$, $P = 2.668 \times 10^{-5}$, $n = 63$) (Fig. 2G). Notably, the total small-spot-evoked inhibitory input (On component + Off component) was significantly correlated ($\rho = 0.480$, $P = 6.992 \times 10^{-5}$, $n = 63$) in amplitude with the optogenetically evoked GAC input to M1as (recorded in the cocktail), consistent with a major contribution of GACs to the light (small spot)-evoked inhibitory input to M1a cells (Fig. 2H). By contrast, we found no significant correlation between small-spot-evoked inward current responses (mainly melanopsin-mediated) and optogenetically evoked GAC inputs ($\rho = 0.038$, $P = 0.768$, $n = 61$) (Fig. 2I), nor did we find a significant correlation between light (small spot)-evoked inward and outward current responses in M1a cells ($\rho = 0.011$, $P = 0.935$, $n = 61$) (Fig. 2J).

Pharmacological experiments further showed that the small spot-evoked On and Off inhibitory inputs to M1a cells were largely blocked by strychnine (63% ± 15% blockade of peak On and 81% ± 9% blockade of peak Off input, $n = 11$), but much less affected by SR (30 ± 17 % blockade of peak On and 11 ± 37 % enhancement of peak Off input, $n = 4$) (Fig. 3A and B), again consistent with a predominantly glycinergic drive from GACs to M1as. Furthermore, the On and Off inhibitory inputs were nearly abolished when M1as were stimulated with a large light spot (575 μm in radius) (Fig. 3C and E), consistent with the previous finding that GACs are completely suppressed by their strong inhibitory surround under the large-spot illumination (Lee *et al.* 2014; Kim *et al.* 2015; Lee *et al.* 2016; Tien *et al.* 2016; Chen *et al.* 2017). By contrast, M1b cells received no or a very weak inhibitory input under small-spot illumination, and their inhibitory responses to large-spot illumination either remained small, or occasionally became slightly enhanced in the On component (Fig. 3D and E). Dual patch clamp recording of neighbouring M1a and M1b cells also confirmed these characteristic differences in inhibitory receptive field structure between the two M1 subtypes ($n = 5$) (Fig. 3F). Taken together, the above results established that M1a, but not M1b, cells possessed a strong centre-inhibitory, surround-disinhibitory receptive field, which was shaped predominantly by the glycinergic input from GACs.

The sbc trigger feature of M1a cells

We next investigated how the receptive field structures of M1a and M1b cells shaped the spike patterns of these cells, as well as whether the inhibitory synaptic input from GACs to M1a cells resulted in any specific visual trigger feature in the response characteristics of M1a cells. On-cell loose-patch recording showed that M1a cells responded to a small centre light spot (50 μm in radius) with a transient suppression of spikes at the light onset and/or offset (Fig. 4A), although such suppression was not observed when the same cells were stimulated by a large spot (500 μm in radius; $n = 19$) (Fig. 4A). This spot size-dependent On-Off spike suppression was reminiscent of the sbc characteristic of uniformity detectors, which have been shown to receive a major glycinergic input from GACs as well (Lee *et al.* 2016; Tien *et al.* 2016). We found the sbc trigger feature to be a robust and characteristic response property of M1a cells (16 out of 19 cells), even though the strength and duration of spike suppression varied from cell to cell (Fig. 4A). On average, a small light spot (50 μm in radius) transiently suppressed 69 ± 39% of the On and 38 ± 36% of the Off spike

rate of M1a cells (n = 19) (Fig. 4C), whereas a large light spot (500 μm in radius) enhanced the On spike rate by 67 ± 158% (n = 19) and slightly suppressed the Off spike rate by 10 ± 9% (n = 8) (Fig. 4C). The small spot-evoked spike suppression was almost abolished by STRY (n = 3) (Fig. 4E), again consistent with an underlying spot size-dependent glycinergic input from GACs. Application of SR (n = 3) on top of STRY further enhanced the initial spike response of M1a cells to a small spot, indicating an additional minor contribution of GABAergic amacrine cells to spike suppression (Fig. 4E).

On the other hand, M1b cells did not display a characteristic sbc trigger feature (Fig. 4B and C). Unlike M1a cells, which typically responded to the onset and/or offset of a small light spot with an initial spike suppression and a subsequent increase in spike rate (Fig. 4A, C and D), M1b cells showed neither a distinctive initial spike suppression, nor a subsequent spike enhancement in response to small-spot illumination (n = 12) (Fig. 4B, C and D). We also occasionally encountered M1b cells that lacked a detectable spike response to either small-or large-spot illumination (two out of 12 cells tested) (Fig. 4B), possibly as a result of heterogeneity within the M1b population and/or special biophysical conditions, such as melanopsin inactivation and depolarization block, although they were indistinguishable from other M1b cells under voltage clamp.

Whole-cell current clamp recording further established that the initial spike suppression seen in the responses of M1a cells to a small (but not large) spot was accompanied by a transient membrane hyperpolarization (n = 30) (Fig. 5A), which was consistent with an inhibitory input from GACs, ruling out the possibility of depolarization block being the source of the suppression. In contrast, M1b cells did not show a transient membrane hyperpolarization in response to a small spot (n = 27) (Fig. 5B), as expected from their lack of a glycinergic input from GACs (Figs 1–3). Notably, the transient kinetics of the small-spot-evoked membrane hyperpolarization in M1a cells (Fig. 5A) resembled the time courses of the spike suppression under on-cell recording (Fig. 4A) and was consistent with the kinetics of both the small-spot-evoked inhibitory synaptic input (Fig. 2) and the direct glycinergic input from optogenetically activated GACs (Fig. 1). This transient kinetics suggested that the sbc trigger feature of M1a cells was tuned to temporally varying and spatially localized contrast signals in the visual field. As shown in Fig. 5C, although a steady (5 s) step change in local contrast produced only a transient spike suppression during the initial ~2 s of the step change, a temporally varying stimulation, such as a train of 1 Hz flashes, could evoke a strong and sustained spike suppression that lasted the entire stimulation duration (10 s). Similarly, a small (but not large) moving light spot also triggered a strong membrane hyperpolarization and spike suppression in M1a cells (n = 4) (Fig. 5D). Thus, the selective glycinergic input from GACs enabled M1a cells to encode dynamic local contrast signals that vary in time and/or space.

Intrinsic differences between M1a and M1b subtypes

In addition to the differences in synaptic connectivity, inhibitory receptive field structure, melanopsin-mediated current amplitude, and receptive field trigger feature between M1a and M1b cells, we also detected differences in intrinsic membrane properties and morphological features between these two M1 subtypes. In response to depolarizing current pulses of

incrementally increasing amplitudes under current clamp recording, M1a cells (n = 34) generated many more spikes than M1b cells (n = 28), although both cell types eventually under-went depolarization block in response to large current injections (Fig. 6A–C). M1a cells (n = 13) also displayed longer total dendritic length (measured in dendritic density) and more dendritic complexity in the central dendritic field than M1b cells (n = 12) (Fig. 6D–F), despite the large variability in dendritic field size and morphology within each of the two M1 subpopulations. On average, the soma diameter of M1a cells was slightly, but statistically significantly, smaller than that of M1b cells (12.9 ± 1.5 μm, n = 72 *vs.* 14.5 ± 1.6 μm, n = 57, $P = 3.14 \times 10^{-8}$). Taken together, our data strongly suggest that M1 cells could be classified into two broad subtypes based on a wide range of distinctively co-varying parameters, including morphology, membrane excitability, intrinsic photosensitivity, synaptic connectivity, receptive field property and functional trigger feature.

Discussion

Synaptic circuitry and receptive-field structure of M1 cells

The above optogenetic, pharmacological and dual patch clamp results have uncovered an unexpected synaptic pathway from GACs to a subpopulation of M1 cells via glycinergic, but not glutamatergic, synapses. This pathway is specific and selective because M1as and uniformity detectors (UDs) are the only two ganglion cell types so far found to receive direct glycinergic input from GACs in our screening of >1000 randomly chosen ganglion cells in the mouse retina, although GACs have also been found to make glycinergic synapses onto a polyaxonal amacrine cell (Jia *et al.* 2020) and glutamatergic synapses onto a few other types of ganglion cells (off alpha, DSGC, W3) (Lee *et al.* 2014; Krishnaswamy *et al.* 2015; Tien *et al.* 2015; Lee *et al.* 2016). Importantly, our results also revealed a complex receptive field structure of M1a cells, including spatiotemporal and pharmacological characteristics consistent with those of GACs, thus supporting a primary role of GACs in shaping the sbc receptive field in both M1a and UD cells, although other amacrine cell types probably provided additional inhibitory inputs. A negative control for this conclusion came from the finding that M1b cells, which received no direct GAC input, lacked both a small-spot-light-evoked inhibitory input and the sbc trigger feature.

The sbc trigger feature of M1a cells and its potential role in vision

Most retinal ganglion cells decrease their responsiveness to a large featureless background in their receptive field. An exception to this rule, however, can be found in UD ganglion cells, for which the spike rates are enhanced by a large uniform field but suppressed by local contrast (Levick, 1967; Rodieck, 1967; Sivyer *et al.* 2010). This sbc trigger feature has been found not only in the retina, but also in image-forming visual centres, such as the dorsal lateral geniculate nucleus (Tailby *et al.* 2007; Piscopo *et al.* 2013), superior colliculus (Ito *et al.* 2017) and visual cortex (Niell & Stryker, 2010). Indeed, the use of the sbc trigger feature to discriminate between visual field uniformity and local contrast is now recognized as a fundamental form of visual processing in image-forming vision (Jacoby & Schwartz, 2018). Interestingly, our results demonstrate that the very same sbc trigger feature is embedded in a subset of non-image-forming M1 cells. M1a cells may use the sbc trigger feature to filter out local and temporally varying contrast signals that

are deleterious to accurate representation of average ambient irradiance. The sbc trigger feature may also be involved in regulating pupillary reflex because a sudden appearance of a small object in the visual field (a light or dark spot) has been reported to draw attention and cause pupil dilation (Wang *et al.* 2014). Although this phenomenon is considered to be mediated largely by the superior colliculus (Wang *et al.* 2014), a sbc-type of suppression of M1a cells and their downstream targets (e.g. OPN) may potentially constitute a more direct underlying mechanism. Likewise, the sbc trigger feature may also enable M1a cells to convey local contrast or contrast-discriminating information to other downstream targets, including the SCN. Intriguingly, a recent study showed that spatial pattern can influence the firing of neurons in SCN (a major target of M1 cells) as much as irradiance can (Mouland *et al.* 2017). SCN has also been reported to mediate behavioural tasks that require image-forming vision, such as socially contagious itch (Yu *et al.* 2017). The present study revealed a retinal circuit for possible cross-talk between imagine-forming (conscious) and non-image-forming (subconscious) visual pathways. How exactly the sbc trigger feature is utilized in non-image-forming visual centres or their downstream targets awaits future study.

M1 cell subtypes

Dendrites of neighbouring M1 cells overlap with a coverage factor of 3.8 (Berson *et al.* 2010), which suggests the potential existence of distinct M1 subtypes based on the retinal mosaic theory (Wassle *et al.* 1981). Although subclassification of M1 cells is supported by the differential expression of molecular markers within the M1 population (Chen *et al.* 2011; Berg *et al.* 2019), there has been little physiological evidence for subtypes within the M1 population based on the biophysical parameters examined so far (Emanuel *et al.* 2017; Milner & Do, 2017). Thus, previous speculations of a diverse functional role of M1 cells in non-image-forming vision were based mainly on M1 projections to various central targets in the brain rather than discrete functional subtypes within the M1 population. Our results now show that M1 cells can be subdivided into two broad functional subgroups based on differential synaptic connectivity with vGluT3 cells and the presence (or lack) of the sbc trigger feature. This synaptic and functional subclassification further allowed us to identify distinctive covariation patterns of several key biophysical and morphological parameters of M1 cells. It remains to be investigated whether there are differences in the central projections of M1a and M1b cells, and whether M1a and M1b subtypes correspond to any of the previously reported M1 subpopulations that differentially express specific genetic markers (Chen *et al.* 2011; Li & Schmidt, 2018; Berg *et al.* 2019) or differentially display certain cellular properties, such as dim light sensitivity and neurotransmitter contents (Lee *et al.* 2019b; Sonoda *et al.* 2020). Based on the number of M1a and M1b cells encountered during our recordings, the ratio of M1a and M1b cells was close to 1:1 (80:73), which did not match the reported ratio of Brn3b-positive and Brn3b-negative M1 cells (14:86 in Chen *et al.* 2011; or 8:92 in Berg *et al.* 2019). It also should be emphasized that future studies of other parameters of M1 cells may possibly identify additional subpopulations within M1a and/or M1b subtypes.

Supplementary Material

Refer to Web version on PubMed Central for supplementary material.

Acknowledgements

The authors thank Xiao-chun Yang, Xun Li, Yu Xiong, and Nannan Yu for technical assistance and In-jung Kim for scientific discussion.

Funding

This work was supported by NIH grant R01 EY026065 (ZJZ), P30 EY026878 (to Yale Vision Core), Marvin L. Sears Endowed Professorship (ZJZ) and the FORE-i Foundation (SL).

Data availability statement

Data will be made available upon reasonable request to the corresponding author.

Biography

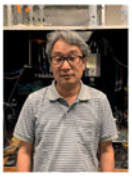

Seunghoon Lee received his PhD in Physiology and Biophysics from University of Arkansas for Medical Sciences, USA in 2005. Currently, he is a Research Scientist in the Department of Ophthalmology and Visual Science at Yale University. His research focuses on synaptic transmission between identified retinal neurons and functional connectivity in retinal circuits, using physiological methods such as dual patch clamp recording, focal laser photolysis, two-photon imaging and optogenetics.

References

Berg DJ, Kartheiser K, Leyrer M, Saali A & Berson DM (2019). Transcriptomic signatures of postnatal and adult intrinsically photosensitive ganglion cells. Eneuro 6, ENEURO.0022–0019.2019.

Berson DM, Castrucci AM & Provencio I (2010). Morphology and mosaics of melanopsin-expressing retinal ganglion cell types in mice. J Comp Neurol 518, 2405–2422. [PubMed: 20503419]

Berson DM, Dunn FA & Takao M (2002). Phototransduction by retinal ganglion cells that set the circadian clock. Science 295, 1070–1073. [PubMed: 11834835]

Chen M, Lee S & Zhou ZJ (2017). Local synaptic integration enables ON-OFF asymmetric and layer-specific visual information processing in vGluT3 amacrine cell dendrites. Proc Natl Acad Sci U S A 114, 11518–11523. [PubMed: 28973895]

Chen SK, Badea TC & Hattar S (2011). Photoentrainment and pupillary light reflex are mediated by distinct populations of ipRGCs. Nature 476, 92–95. [PubMed: 21765429]

Dacey DM, Liao HW, Peterson BB, Robinson FR, Smith VC, Pokorny J, Yau KW & Gamlin PD (2005). Melanopsin-expressing ganglion cells in primate retina signal colour and irradiance and project to the LGN. Nature 433, 749–754. [PubMed: 15716953]

Ecker JL, Dumitrescu ON, Wong KY, Alam NM, Chen SK, LeGates T, Renna JM, Prusky GT, Berson DM & Hattar S (2010). Melanopsin-expressing retinal ganglion-cell photoreceptors: cellular diversity and role in pattern vision. Neuron 67, 49–60. [PubMed: 20624591]

Emanuel AJ, Kapur K & Do MTH (2017). Biophysical variation within the M1 Type of ganglion cell photo-receptor. Cell Rep 21, 1048–1062. [PubMed: 29069587]

Gooley JJ, Lu J, Chou TC, Scammell TE & Saper CB (2001). Melanopsin in cells of origin of the retinohypothalamic tract. Nat Neurosci 4, 1165. [PubMed: 11713469]

Grimes WN, Seal RP, Oesch N, Edwards RH & Diamond JS (2011). Genetic targeting and physiological features of VGLUT3+ amacrine cells. Vis Neurosci 28, 381–392. [PubMed: 21864449]

Hannibal J, Hindersson P, Knudsen SM, Georg B & Fahrenkrug J (2002). The photopigment melanopsin is exclusively present in pituitary adenylate cyclase-activating polypeptide-containing retinal ganglion cells of the retinohypothalamic tract. J Neurosci 22, RC191. [PubMed: 11756521]

Hattar S, Liao HW, Takao M, Berson DM & Yau KW (2002). Melanopsin-containing retinal ganglion cells: architecture, projections, and intrinsic photosensitivity. Science 295, 1065–1070. [PubMed: 11834834]

Ito S, Feldheim DA & Litke AM (2017). Segregation of visual response properties in the mouse superior colliculus and their modulation during locomotion. J Neurosci 37, 8428–8443. [PubMed: 28760858]

Jacoby J & Schwartz GW (2018). Typology and circuitry of suppressed-by-contrast retinal ganglion cells. Front Cell Neurosc 12, 269.

Jia Y, Lee S, Zhuo Y & Zhou ZJ (2020). A retinal circuit for the suppressed-by-contrast receptive field of a polyaxonal amacrine cell. Proc Natl Acad Sci U S A 117, 9577–9583. [PubMed: 32273387]

Kim T & Kerschensteiner D (2017). Inhibitory control of feature selectivity in an object motion sensitive circuit of the retina. Cell Rep 19, 1343–1350. [PubMed: 28514655]

Kim T, Soto F & Kerschensteiner D (2015). An excitatory amacrine cell detects object motion and provides feature-selective input to ganglion cells in the mouse retina. eLife 4, e08025.

Krishnaswamy A, Yamagata M, Duan X, Hong YK & Sanes JR (2015). Sidekick 2 directs formation of a retinal circuit that detects differential motion. Nature 524, 466–470. [PubMed: 26287463]

Lee S, Chen L, Chen M, Ye M, Seal RP & Zhou ZJ (2014). An unconventional glutamatergic circuit in the retina formed by vGluT3 amacrine cells. Neuron 84, 708–715. [PubMed: 25456497]

Lee S, Chen M, Shi Y, Yang X & Zhou Z (2019a). GLycinergic supression of a M1-ipRGC subpopulation by vGluT3 amacrine cells in the mouse retina. Invest Ophthalmol Vis Sci 60, 1375.

Lee S, Kim K & Zhou ZJ (2010). Role of ACh-GABA cotransmission in detecting image motion and motion direction. Neuron 68, 1159–1172. [PubMed: 21172616]

Lee S, Zhang Y, Chen M & Zhou ZJ (2016). Segregated glycine-glutamate co-transmission from vGluT3 amacrine cells to contrast-suppressed and contrast-enhanced retinal circuits. Neuron 90, 27–34. [PubMed: 26996083]

Lee SK, Sonoda T & Schmidt TM (2019b). M1 intrinsically photosensitive retinal ganglion cells integrate rod and melanopsin inputs to signal in low light. Cell Rep 29, 3349–3355 e3342. [PubMed: 31825819]

Levick WR (1967). Receptive fields and trigger features of ganglion cells in the visual streak of the rabbits retina. J Physiol 188, 285–307. [PubMed: 6032202]

Li JY & Schmidt TM (2018). Divergent projection patterns of M1 ipRGC subtypes. J Comp Neurol 526, 2010–2018. [PubMed: 29888785]

Lucas RJ, Douglas RH & Foster RG (2001). Characterization of an ocular photopigment capable of driving pupillary constriction in mice. Nat Neurosci 4, 621–626. [PubMed: 11369943]

Milner ES & Do MTH (2017). A population representation of absolute light intensity in the mammalian retina. Cell 171, 865–876 e816. [PubMed: 28965762]

Mouland JW, Stinchcombe AR, Forger DB, Brown TM & Lucas RJ (2017). Responses to spatial contrast in the mouse suprachiasmatic nuclei. Curr Biol 27, 1633–1640 e1633. [PubMed: 28528901]

Niell CM & Stryker MP (2010). Modulation of visual responses by behavioral state in mouse visual cortex. Neuron 65, 472–479. [PubMed: 20188652]

Panda S, Sato TK, Castrucci AM, Rollag MD, DeGrip WJ, Hogenesch JB, Provencio I & Kay SA (2002). Melanopsin (Opn4) requirement for normal light-induced circadian phase shifting. Science 298, 2213–2216. [PubMed: 12481141]

Perez-Leon JA, Warren EJ, Allen CN, Robinson DW & Brown RL (2006). Synaptic inputs to retinal ganglion cells that set the circadian clock. Eur J Neurosci 24, 1117–1123. [PubMed: 16930437]

Piscopo DM, El-Danaf RN, Huberman AD & Niell CM (2013). Diverse visual features encoded in mouse lateral geniculate nucleus. J Neurosci 33, 4642–4656. [PubMed: 23486939]

Provencio I, Rollag MD & Castrucci AM (2002). Photo-receptive net in the mammalian retina. This mesh of cells may explain how some blind mice can still tell day from night. Nature 415, 493.

Rodieck RW (1967). Receptive fields in the cat retina: a new type. Science 157, 90–92. [PubMed: 6026674]

Ruby NF, Brennan TJ, Xie X, Cao V, Franken P, Heller HC & O'Hara BF (2002). Role of melanopsin in circadian responses to light. Science 298, 2211–2213. [PubMed: 12481140]

Schmidt TM & Kofuji P (2009). Functional and morphological differences among intrinsically photosensitive retinal ganglion cells. J Neurosci 29, 476–482. [PubMed: 19144848]

Schmidt TM, Taniguchi K & Kofuji P (2008). Intrinsic and extrinsic light responses in melanopsin-expressing ganglion cells during mouse development. J Neurophysiol 100, 371–384. [PubMed: 18480363]

Sivyer B, Taylor WR & Vaney DI (2010). Uniformity detector retinal ganglion cells fire complex spikes and receive only light-evoked inhibition. Proc Natl Acad Sci U S A 107, 5628–5633. [PubMed: 20212117]

Sonoda T, Li JY, Hayes NW, Chan JC, Okabe Y, Belin S, Nawabi H & Schmidt TM (2020). A noncanonical inhibitory circuit dampens behavioral sensitivity to light. Science 368, 527–531. [PubMed: 32355031]

Tailby C, Solomon SG, Dhruv NT, Majaj NJ, Sokol SH & Lennie P (2007). A new code for contrast in the primate visual pathway. J Neurosci 27, 3904–3909. [PubMed: 17409255]

Tien NW, Kim T & Kerschensteiner D (2016). Target-specific glycinergic transmission from VGluT3-expressing amacrine cells shapes suppressive contrast responses in the retina. Cell Rep.

Tien NW, Pearson JT, Heller CR, Demas J & Kerschensteiner D (2015). Genetically identified suppressed-by-contrast retinal ganglion cells reliably signal self-generated visual stimuli. J Neurosci 35, 10815–10820. [PubMed: 26224863]

Wang CA, Boehnke SE, Itti L & Munoz DP (2014). Transient pupil response is modulated by contrast-based saliency. J Neurosci 34, 408–417. [PubMed: 24403141]

Wassle H, Peichl L & Boycott BB (1981). Dendritic territories of cat retinal ganglion cells. Nature 292, 344–345. [PubMed: 7254331]

Wong KY, Dunn FA & Berson DM (2005). Photoreceptor adaptation in intrinsically photosensitive retinal ganglion cells. Neuron 48, 1001–1010. [PubMed: 16364903]

Wong KY, Dunn FA, Graham DM & Berson DM (2007). Synaptic influences on rat ganglion-cell photoreceptors. J Physiol 582, 279–296. [PubMed: 17510182]

Yu YQ, Barry DM, Hao Y, Liu XT & Chen ZF (2017). Molecular and neural basis of contagious itch behavior in mice. Science 355, 1072–1076. [PubMed: 28280205]

Zhao X, Stafford BK, Godin AL, King WM & Wong KY (2014). Photoresponse diversity among the five types of intrinsically photosensitive retinal ganglion cells. J Physiol 592, 1619–1636. [PubMed: 24396062]

Key points

- M1 intrinsically photosensitive retinal ganglion cells (ipRGCs) are known to encode absolute light intensity (irradiance) for non-image-forming visual functions (subconscious vision), such as circadian photoentrainment and the pupillary light reflex.
- It remains unclear how M1 cells respond to relative light intensity (contrast) and patterned visual signals.
- The present study identified a special form of contrast sensitivity (suppressed-by-contrast) in M1 cells, suggesting a role of patterned visual signals in regulating non-image-forming vision and a potential role of M1 ipRGCs in encoding image-forming visual cues.
- The study also uncovered a synaptic mechanism and a retinal circuit mediated by vesicular glutamate transporter 3 (vGluT3) amacrine cells that underlie the suppressed-by-contrast response of M1 cells.
- M1 ipRGC subtypes (M1a and M1b) were revealed that are distinguishable based on synaptic connectivity with vGluT3 amacrine cells, receptive field properties, intrinsic photo sensitivity and membrane excitability, and morphological features, suggesting a division of visual tasks among discrete M1 subpopulations.

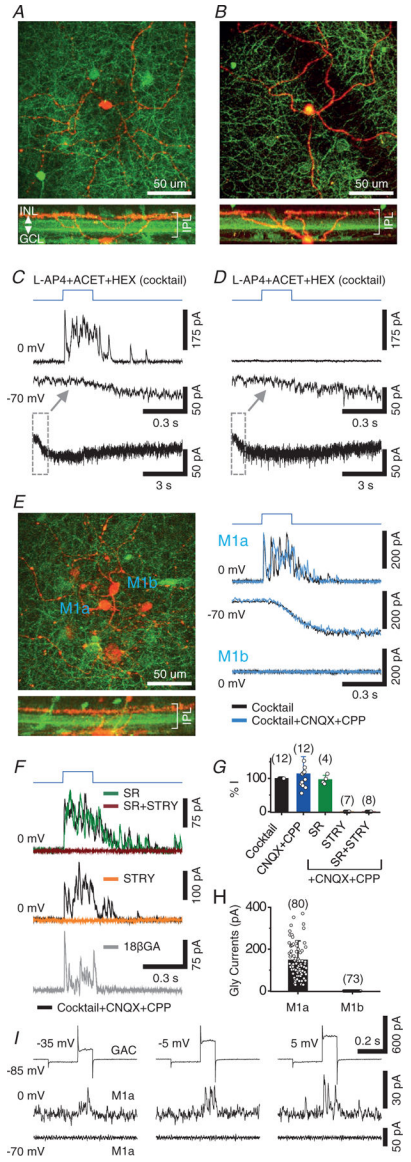

Figure 1. Selective glycinergic transmission from GACs to a subpopulation of M1 ipRGCs

A, maximum z-projection (top) and cross-sectional reconstruction (bottom) of a two-photon image stack taken from a recorded M1 cell (red, Alexa 594) in a OPN4-GFP/vGluT3Cre/ChR2-YFP (green) retina. *B*, another example of a M1 cell. *C*, voltage clamp recording of the M1 cell in (*A*) in the presence of a control cocktail, showing fast outward postsynaptic currents at 0 mV (~E_{cat}) and slow melanopsin-mediated inward currents at −70 mV (~E_{cl}) in response to optogenetic activation of GACs by full-field *blue light* (blue trace). Bottom: slow inward currents on a longer time scale. *D*, voltage clamp recording of the M1 cell in (*B*), showing slow inward current at −70 mV, but no outward current at 0 mV. *E*, dual patch clamp recording of two adjacent M1 cells in the presence of control cocktail, showing robust outward postsynaptic currents in M1a cell (top), but no current in M1b cell (bottom), at 0 mV in response to optogenetic activation of GACs. The outward (top) and inward current (at −70 mV, middle) responses in M1a cell were resistant to CNQX (40 μM) +

CPP (20 μM). *F*, top, middle: strychnine (STRY) (1–2 μM), but not gabazine (SR95531) (50 μM), completely abolished the outward responses of M1a cells at 0 mV in the cocktail + CNQX (40 μM) + CPP (20 μM). This optogenetically evoked glycinergic response in the cocktail remained largely intact after 15- to 25-min perfusion of 18 β-GA (bottom, 25 μM). *G*, summary of pharmacological effects on *blue light* (ChR2)-evoked peak outward currents (at 0 mV) in M1a cells. *H*, comparison of blue-light (ChR2)-evoked glycinergic current between M1a and M1b cells. *I*, dual patch clamp recording from a pair of GAC and M1a, showing voltage-gated currents of GAC (top) in response to depolarizing steps (100 ms long, preceded by 200 ms long pre-step from −85 mV to −100 mV) and outward postsynaptic current responses at 0 mV (middle), but no postsynaptic response at −70 mV (bottom), in the M1a cell. Values in parentheses indicate the number of cells tested. Error bars represent the SD. Cocktail concentrations: L-AP4 (20 μM), ACET (20 μM) and HEX (300 μM).

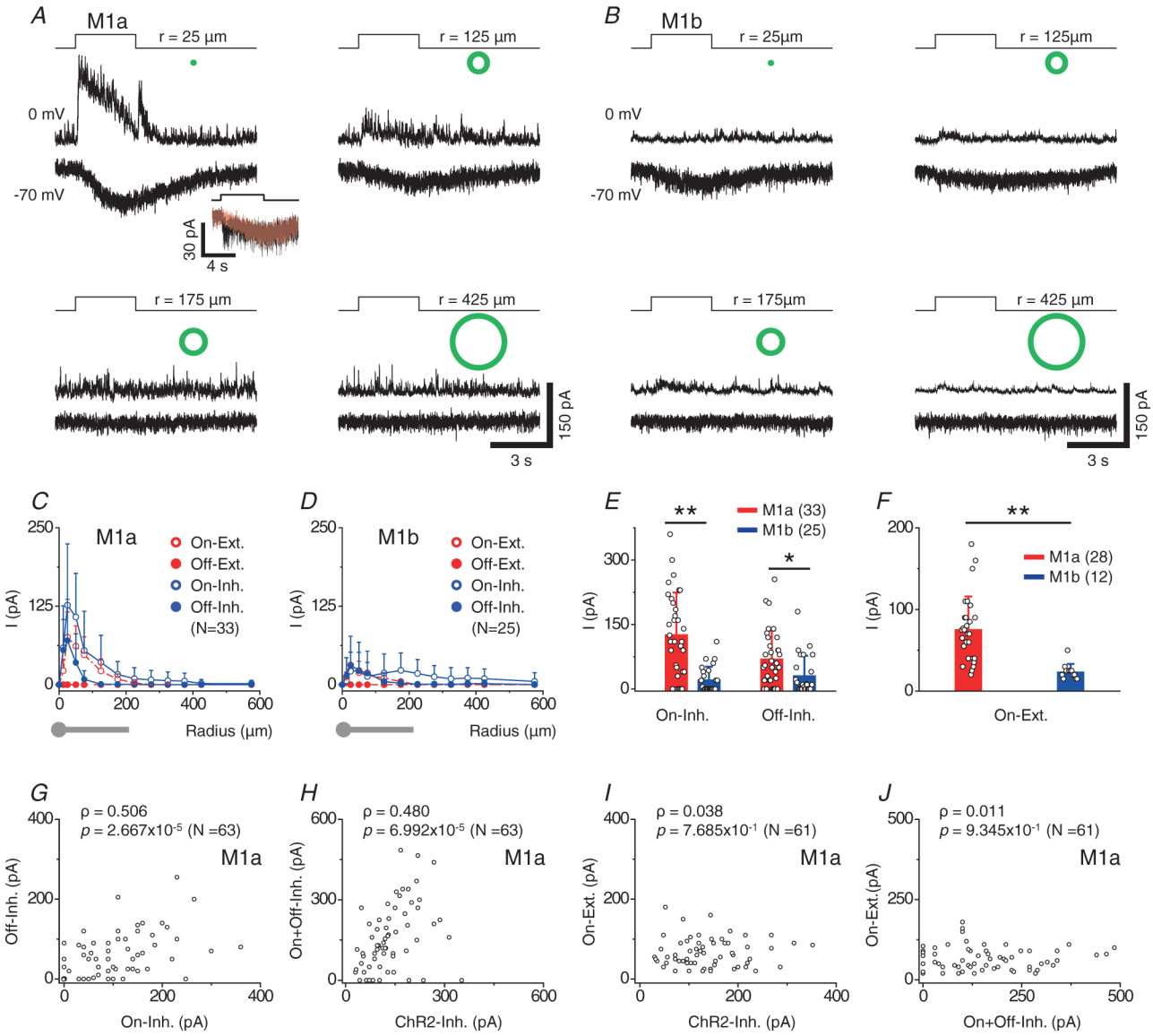

Figure 2. Receptive field properties of M1a and M1b cells

A and *B*, excitatory (at −70 mV) and inhibitory (at 0 mV) currents of a M1a (*A*) and a M1b cell (*B*) to flashes of white light annuli (green symbols) of various radii (*r*, defined as the mean of inner and outer radii). All annuli were 50 µm thick except for the smallest one (25 µm thick) (*A*, inset, another M1a cell). An initial transient excitatory component was occasionally seen on top of the slow inward current in response to a light spot of 50-µm radius at −70 mV, and it could be blocked by L-AP4 (10 µM, red). *C* and *D*, peak excitatory and inhibitory currents of M1a (*C*) and M1b cells (*D*) as a function of annulus radius. Drawings below the graphs show average dendritic size (radius) of M1 cells (grey). *E*, comparison of maximum On and Off inhibitory postsynaptic currents (typically evoked by small light annuli of 25–50 µm in radius) between M1a and M1b cells. Statistical significance: $*P = 1.40 \times 10^{-2}$ and $**P = 3.05 \times 10^{-6}$ (student's two sample *t* test). [Correction made on 15 November 2021, after first online publication: The precise *P* values have been inserted in the preceding sentence]. *F*, summary of maximum

excitatory currents (typically evoked by small light annuli of 25–50 μm in radius and mainly mediated by melanopsin). Statistical significance: $^{**}P = 9.18 \times 10^{-5}$ (Student's two sample *t* test). [Correction made on 15 November 2021, after first online publication: The precise *P* values have been inserted in the preceding sentence.] *G–J*, correlation analyses of annuli (25–50 μm in radius)-evoked inhibitory synaptic currents (denoted as On- and Off-inhibition), optogenetically evoked inhibitory currents (shown as ChR2-Inh) and annuli-evoked excitatory currents (shown as On-excitation, largely mediated by melanopsin) in M1a cells. Positive correlation was found between On- and Off-inhibition (*G*) and between total (On+Off) inhibition and ChR2-inhibition (*H*), but not between On-excitation and ChR2-inhibition (*I*) or between On-excitation and total (On+Off) inhibition (*J*). Spearman's correlation coefficients (ρ) and associated *P* values are shown. Values in parentheses indicate the number of cells tested. Error bars represent SD.

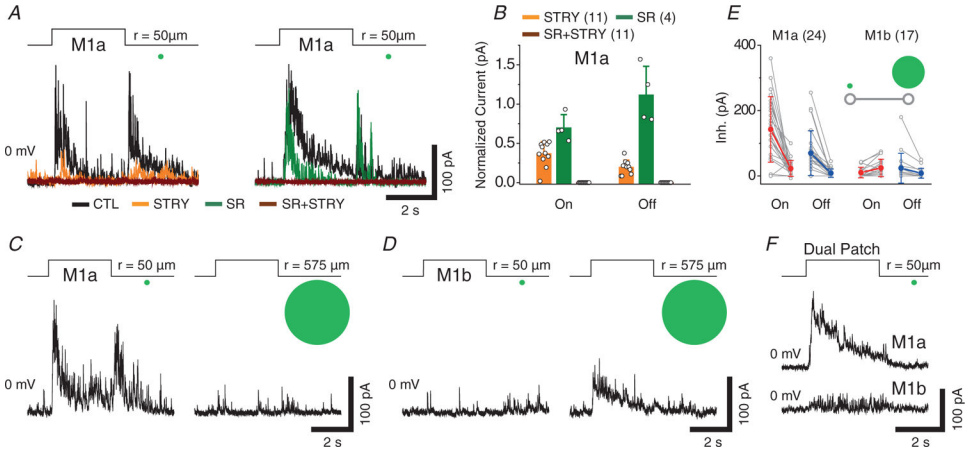

Figure 3. Characterization of light spot-evoked inhibitory inputs to M1a and M1b cells

A, effects of STRY (1 μM) and SR (50 μM) on the inhibitory responses (at 0 mV) of M1as to centre light spot (50 μm in radius). *B*, summary of pharmacological effects on centre light spot-evoked peak inhibitory currents in M1a cells. *C* and *D*, large light spot (575 μm in radius) suppressed On- and Off-inhibitory responses in M1a cells (*C*), but induced small On-inhibitory responses in M1b cells (*D*). *E*, comparison of inhibitory currents evoked by centre and large light spot between M1a and M1b cells. Inset: line-connected data pair represents peak inhibitory responses to small and large light spot. *F*, an example of dual patch clamp recording of neighbouring (~50 μm apart) M1a and M1b cells, showing strong inhibitory current response to centre light spot (50–100 μm in radius, positioned between them) in the M1a, but little response in the M1b cell. Values in parentheses indicate the number of cells tested. Error bars indicate the SD.

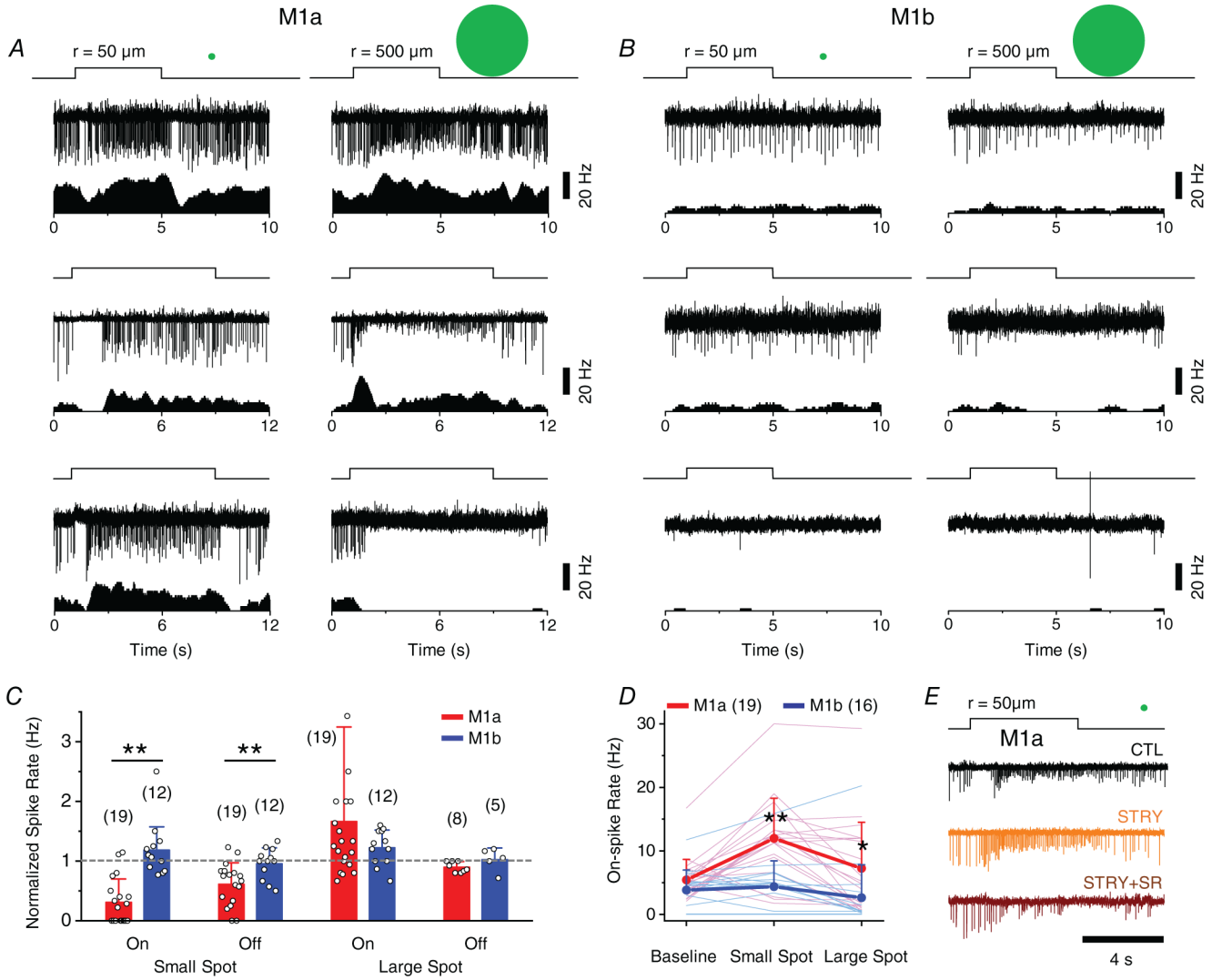

Figure 4. Suppressed-by-contrast receptive field properties of M1a cells

A, spike responses (upper) and associated rate plots (lower) of three examples of M1a cells to flashes of a small (50 µm in radius, left) and a large (500 µm in radius, right) light spot under on-cell loose-patch recording, showing a transient suppression of tonic background spikes at the onset and/or offset of the small spot (left), but not the large (right) spot. Note that the lack of transient suppression by the large spot was often followed by a long-lasting reduction in spike amplitude and, in severe cases, complete cessation of spikes, presumably due to depolarization block (a well-known phenomenon with M1 cells). *B*, spike responses and associated rate plots of three examples of M1b cells, showing a lack of transient suppression by either a small (left) or a large light spot (right) at light onset or offset. Note that M1b cells also frequently displayed slowly activating and long-lasting depolarization block in response to a large spot (middle) and, occasionally, were found to give little or no light response (bottom). *C*, summary of transient modulations of M1a and M1b spike rates by small and large light spots (normalized to baseline spike rate), measured during a 0.5 s period starting at 0.5 s after the onset and offset of light spot. Cells with strong depolarization block (11 out of 19 M1a cells and seven out of 12 M1b cells) were excluded

from the analysis of Off responses to a large spot. *P* values for each paired data from left to right were 4.29×10^{-6}, 8.21×10^{-3}, 0.307 and 0.137, respectively. *D*, comparison of mean spike rates between M1a and M1b cells at the background level and during the entire period of illumination with small and large spots, showing significantly higher spike rates in M1a than in M1b cells for both small ($P = 2.06 \times 10^{-4}$) and large ($P = 0.0392$) spots. *E*, effects of STRY (1 μM) and STRY (1 μM) + SR (50 μM) on small-spot-evoked transient spike suppression in M1a cells. Values in parentheses indicate the number of cells tested. Error bars indicate the SD. Statistical significance: $*P < 0.05$ and $**P < 0.01$ (Student's two sample *t* test).

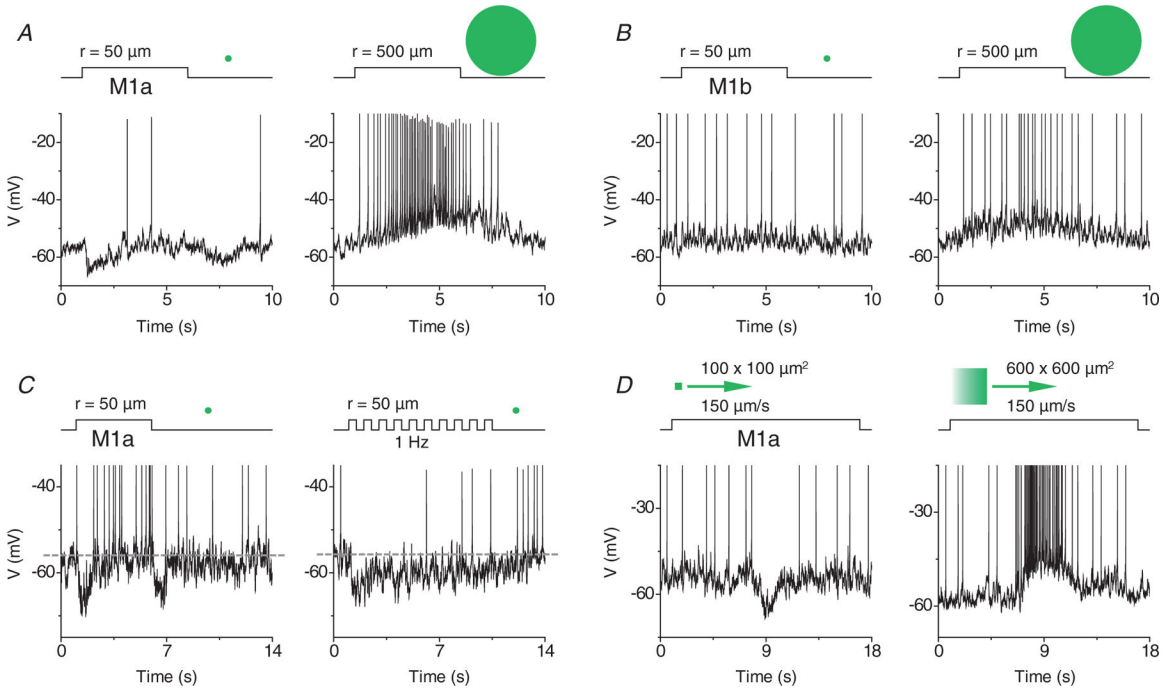

Figure 5. Hyperpolarization of membrane potential underlies suppressed-by-contrast receptive field property of M1a cells

A, current clamp recordings of a M1a cell, showing transient hyperpolarization induced by a small (left), but not large (right), light spot at light onset and offset. *B*, neither small (left), nor large (right), light spot evoked detectable hyperpolarization in a M1b cell. *C*, temporal properties of spike suppression in M1a cells, showing transient On/Off hyperpolarization and spike suppression by a steady small spot (left), and sustained hyperpolarization and spike suppression by a temporally varying small spot (1 Hz flicker, right). *D*, hyperpolarization and spike suppression induced in a M1a cell by a small (100 × 100 μm^2), but not large (600 × 600 μm^2), moving light spot (150 $\mu m\ s^{-1}$). All recordings (*A*–*D*) were made in I = 0 mode.

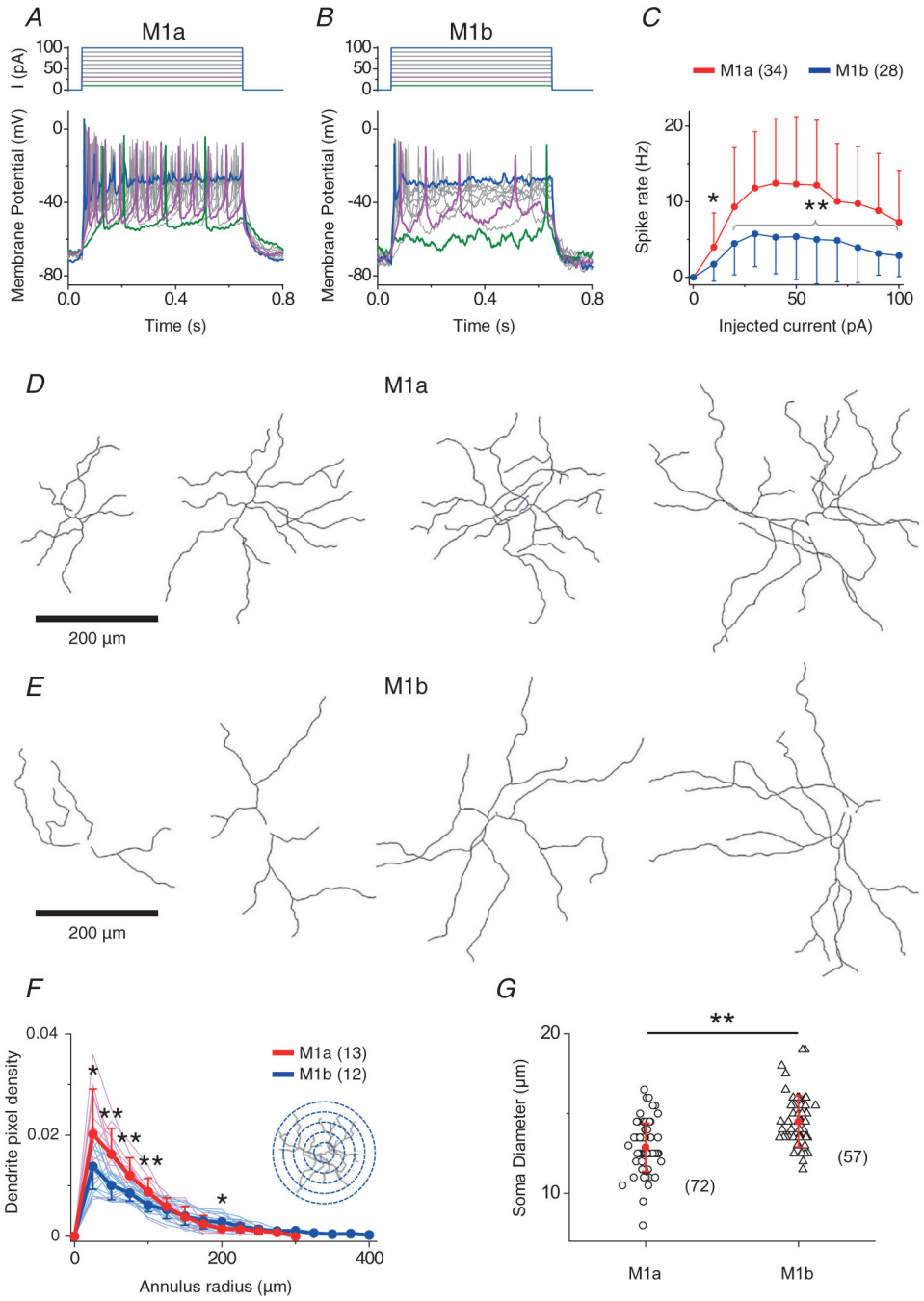

Figure 6. Biophysical and morphological differences between M1a and M1b cells

A and *B*, responses of M1a (*A*) and M1b (*B*) cells to depolarizing current steps under current clamp, showing much more spikes evoked in M1a cells than in M1b cells. Note that both M1a and M1b cells eventually displayed depolarization block in response to large current injections. *C*, spike rate as a function of current step amplitude for M1a and M1b cells. Statistical significance: $*P = 2.1 \times 10^{-2}$ and $**P = 4.0 \times 10^{-3}$, 4.1×10^{-4}, 2.2×10^{-4}, 9.0×10^{-4}, 4.5×10^{-4}, 5.0×10^{-3}, 8.3×10^{-4}, 5.6×10^{-4}, and 2.0×10^{-3} (from left to right). [Correction made on 15 November 2021, after first online publication: The precise *P*

values have been inserted in the preceding sentence.] *D* and *E*, examples of binary images of recorded M1a and M1b cells, showing a more complex and dense dendrite structure of M1a than that of M1b cells in central region. Scale bars = 200 μm. *F*, pixel density of M1a and M1b dendrites, defined as the number of pixels occupied by dendrites within an annulus area (radius *r*, 25 μm-thick, centred on the soma, seen in inset) divided by total number of pixels in the annulus area. Statistical significance: $*P = 0.036$ and 0.028 (left and right, respectively) and $**P = 0.001$, 0.004, 0.006 (from left to right). [Correction made on 15 November 2021, after first online publication: The precise *P* values have been inserted in the preceding sentence.] *G*, summary of soma size between M1a and M1b cells. Statistical significance: $**P = 3.1 \times 10^{-8}$ [Correction made on 15 November 2021, after first online publication: The precise *P* values have been inserted in the preceding sentence.] Values in parentheses indicate the number of cells tested. Error bars indicate the SD.